

We are IntechOpen, the world's leading publisher of Open Access books Built by scientists, for scientists

6,900

Open access books available

186,000

International authors and editors

200M

Downloads

Our authors are among the

154

Countries delivered to

TOP 1%

most cited scientists

12.2%

Contributors from top 500 universities



WEB OF SCIENCE™

Selection of our books indexed in the Book Citation Index
in Web of Science™ Core Collection (BKCI)

Interested in publishing with us?
Contact book.department@intechopen.com

Numbers displayed above are based on latest data collected.
For more information visit www.intechopen.com



Algorithms for Automatic, Real-Time Tsunami Detection in Sea Level Measurements

Gian Mario Beltrami, Marcello Di Risio and Paolo De Girolamo
*DISAT-LIAM - Università di L'Aquila
Italy*

1. Introduction

Automatic, real-time tsunami detection in sea-level measurements is a main component of a tsunami early warning system (TEWS). Although a great effort has been recently undertaken by the scientific and engineering community in developing new technologies (e.g. satellite altimetry, detectors of low-frequency elastic oscillations associated to a tsunami) capable of increasing the awareness of potential tsunamis in the minimum amount of time, at present direct detection in sea level measurements is still the main mean to confirm their actual generation and propagation.

Clearly, the device used to collect these measurements has to be chosen between those equipped with sensors capable of detecting sea-level oscillations within the tsunami frequency band. At present, the main devices that can be actually used should belong to the following classes:

- i) Bottom pressure recorders (BPRs), or tsunamometers;
- ii) Tidal gauges (TGs); and
- iii) Wind-wave gauges (WWGs) equipped with either pressure, or acoustic, or optical sensors.

As far as the third class is concerned, it is to be noticed that tsunami detection cannot be performed by an accelerometric 'wave buoy', i.e. the main device used to collect wind wave measurements. Actually, a buoy is not capable of detecting the propagation of very long waves such tsunamis.

As a general rule, the choice of the device to be effectively used mainly depends on its operational location. This location should be determined on the basis of a tsunami hazard assessment (i.e. a previous knowledge both of probable tsunami sources and of places at risk along the coast). To be effective, measurements should be collected either in close proximity of probable tsunami sources, or between these sources and the coast at risk (at a distance from the coast capable of guaranteeing timely warning of actually approaching tsunamis). For the purpose of the present chapter, the probable tsunami sources can be listed on the basis of their location with respect to the coast of interest, i.e.:

- i) sources located far away from the coast (at a distance on the order of thousands of kilometers);
- ii) sources located at the coast; and

- iii) sources located 'near' the coast (at a distance ranging from tens to few hundreds of kilometers).

When the tsunami sources are far away from the coast of interest, it will be convenient to collect sea-level measurements far out at sea, between these sources and the coast at risk. Such a location implies great water depths, and makes bottom pressure recorders (BPRs) with autonomous power supply the more suitable devices to be used. A BPR (Eble & Gonzalez, 1991) actually measures pressure fluctuations indirectly by evaluating the vibrational variations that these fluctuations cause in a quartz-bean piezometrically induced to oscillate in its lowest resonant flexural mode. Its sampling interval is generally set equal to 15 s. Such a technology makes possible to locate the device on the sea floor, at water depths ranging from hundreds to some thousands of meters (i.e. at water depths at which only pressure fluctuations induced by propagating waves within the tsunami and tidal frequency band can be detected). These characteristics gain BPR the name of *tsunamometer*, and make it undoubtedly the more suitable device to confirm the propagation towards a coast of a tsunami generated far out at sea by either an earthquake, or a submarine landslide, or the eruption of a submerged volcano, or a meteorite impacting the ocean. Indeed, wind-wave gauges (WWGs) mounted above or below mean sea level (at a distance from it around 10 m) on preexisting offshore platforms may also be used in this case, depending on the platform distance from the coast of interest. These devices can be equipped with either pressure, or acoustic, or optical sensors, and usually collect measurements at a sampling frequency equal to 2 Hz. If the sea surface is continuously monitored, these devices will be perfectly able to detect a tsunami.

When tsunamis may be generated at the coast of interest (either by landslides, or coastal earthquakes, or coastal volcano eruptions), it will be essential to collect sea-level measurements in close proximity of the sources. Such a location implies water depths in the order of tens of meters, and makes WWGs such as the standard pressure transducers (SPTs) a suitable and economically convenient choice. In this case, a further important issue will be whether or not the source distance from the closest inhabited location makes the elapsed time between the tsunami generation and arrival sufficient to provide a warning. An example is given by the island of Stromboli, in the southern part of the Tyrrhenian Sea (Italy). On December 30, 2002 two tsunamis were generated by landslides detached from the 'Sciara del Fuoco' on the north-west flank of the volcano of Stromboli (Tinti et al., 2003). The tsunamis propagated both towards the coasts of Sicily, and around the island, hitting the village of Stromboli few minutes after their generation. The landslides and the tsunamis represented the most threatening episodes of a strong eruption started on December 28. In spite of the intensified seismic monitoring carried out in response to the eruption, nor the landslides nor the tsunamis were foreseen. Following these events, the 'Dipartimento della Protezione Civile', DPC (Italian Civil Protection Department), set up a specific TEWS which relies on real-time monitoring not only of the volcano seismic activity (e.g. Langer & Falsaperla, 2003), but also of the 'Sciara del Fuoco' ground movements (e.g. Corsini et al., 2003), and of sea-level oscillations. In particular, two land-cabled SPTs with a sampling frequency equal to 2 Hz were initially deployed in the sea at the two sides of the 'Sciara del Fuoco'. Both SPTs lay on the sea bottom at a water depth around ten meters. At present, sea-level oscillations are monitored by a SPT installed at a depth equal to 14 m on an elastic beacon deployed in the sea opposite the 'Sciara del Fuoco' at a water depth equal to 43 m.

When tsunamis may be generated 'near' the coast of interest, the main problem won't be the type and the location of the device used for detection. The main problem will be whether or not the source distance from the coast of interest makes the elapsed time between the

tsunami generation and arrival sufficient to provide a warning. The celerity of tsunamis is on the order of hundreds of kilometers per hour, so a time-window around some tens of minutes will be available for a warning in the case of a tsunami generated few hundreds of kilometers away, whilst a tsunami generated some tens of kilometers offshore will impact the adjacent coast in minutes. In the first case, either specifically deployed BPRs or WWGs mounted on opportunely located preexisting offshore platforms can be effectively included in a TEWS. As far as the second case is concerned, the only chance is that, due to the frequency dispersion of the tsunami, the time elapsed between the arrival of its leading wave and its peak amplitude (McGehee & McKinney, 1996) would be sufficient to provide some degree of warning. Either SPTs or other coastal WWGs (mounted on either elastic beacons or preexisting offshore platforms) should be use in this case.

Whatever the sensor type and location, the optimal use of sea-level measurements depends on the effectiveness of the detection algorithm implemented in the software of the sensor. It has been recognized (Beltrami, 2008) that the requisites for an effective algorithm can be identified as:

- a) an ability to discriminate a tsunami from other sea-level oscillations that, falling within the frequency band detected by the sensor, are 'disturbances' in the context of tsunami detection;
- b) an ability to identify the waveform of a tsunami and to characterize it in terms of both amplitude and period; and
- c) a fast computational time.

In the case of BPRs, a fourth requisite should also be considered and met (Beltrami, 2008). Owing to their location, these sensors must have an autonomous power supply. Therefore, the algorithm should run with the lowest possible power consumption. Such a requisite has not necessarily to be met by an algorithm implemented in the software of either a WWG or a tidal gauge. Near-shore SPTs and WWGs located either on offshore platforms or elastic beacons, as well as tidal gauges, can actually be connected to a source of power by a cable. It is furthermore to be noticed that the characteristics of the algorithm may also depend on the apparatus for device to land data transmission.

As far as requisite (a) is concerned, it should be noted that only filtering out non tsunami waves makes it possible to monitor the actual propagation of a tsunami by checking either the amplitude (*amplitude-discriminating algorithm*) or the slope (*slope-discriminating algorithm*) of the recorded signal against a prescribed threshold. Indeed, the presence of several frequencies in a sensor recorded signal guarantees the instrument's polifunctionality. It is in-fact economically desirable to have a device that can measure the wider range of oscillation phenomena.

While the 'disturbance' recorded by a BPR is caused by the superposition of actual sea-surface fluctuations (e.g. planetary waves, astronomical and meteorological tides, gravitational normal modes) and background sea noise (Mofjeld, 1997; Beltrami, 2008), several other 'disturbances' may affect WWG measurements (Beltrami & De Girolamo, 2006). In addition to the above listed wave patterns and to wind waves (for detecting which these sensors are designed), a near-shore WWG can actually measure infragravity waves (e.g. bound/free-long waves, edge waves, surf beats).

It has been shown (Mofjeld, 1997; Beltrami, 2008) that the 'disturbance' recorded by a BPR can be closely predicted, making possible to filter it out simply by subtracting the values observed from those predicted. On the contrary, a close prediction of a wind-wave signal

is not possible, therefore some form of low-pass digital filter has to be implemented in the tsunami detection algorithm of a WWG in order to filter out these waves. It is well known (e.g. Emery & Thomson, 2001), that an effective low-pass digital filter should possess five, often mutually exclusive, essential qualities:

- 1) a sharp cut-off, so that unwanted high-frequency components are effectively removed;
- 2) a comparatively flat pass-band that leaves the low frequencies unchanged;
- 3) a clean transient response so that rapid changes in the signal do not result in spurious oscillation or 'ringing' within the filtered record;
- 4) a zero phase shift; and
- 5) an acceptable computational time.

A sixth requisite should also be met in the context of automatic, real-time tsunami detection. The filter to be used should belong to the class of causal or physically realizable filters, i.e. to the class of filters that use as input only actually available or 'past' signal samples. It is to be noticed that the use of only 'past' samples makes a zero-phase response not possible for causal filters. A way to get round this problem is to design a filter that has, at least, a linear phase response, i.e. a symmetrical impulse response with location of symmetry shifted from the sample to be filtered. In-fact, since this shift does nothing but produce an identical shift in the output signal, a linear phase filter is equivalent to a zero phase one for most purposes (e.g. Smith, 1997; Sheno, 2006). It is finally to be stressed that, in the context of real-time tsunami detection, the time-domain approach to filter design undoubtedly possesses the appealing pro of making the filtered signal immediately available.

At present, two algorithms expressly designed to detect a tsunami in real-time within a BPR recorded signal have been already published: the one developed by Mofjeld (1997) under the NOAA's DART program; and that proposed by Beltrami (2008). These algorithms use a cubic polynomial and an artificial neural network respectively in order to closely predict and filter out the 'disturbance' recorded by a BPR. Currently, two further algorithms are being developed (Pignagnoli et al., 2010; Tinti et al., 2009; Bressan & Tinti, 2010). These last algorithms have been presented at the EGU General Assembly 2010, but have not been published yet.

As far as algorithms designed to detect a tsunami within a WWG's signal are concerned, those already published are that developed by McGehee & McKinney (1996), that used by the Italian Department for Civil Protection (DPC) within the Stromboli's TEWS (Leva, 2004), and that developed by the Port and Airport Research Institute of Japan - PARI (Shimizu et al., 2006; Nagai & Shimizu, 2009). While the first two algorithms are based on a cascade of time domain moving average filters, the third one uses a finite impulse response (FIR) time domain filter (TDF). The algorithm by McGehee & McKinney (1996) and by PARI (Shimizu et al., 2006) are suitable for automatic, real-time detection of tsunamis with periods greater than 10 minutes. On the other hand, that by DPC is limited by its poor performance in removing wind-waves. In order to overcome the constraints of the preceding listed algorithms Beltrami & Di Risio (2010) have developed a new algorithm based on a cascade of causal filters, the main one being an infinite impulse response (IIR) time domain digital filter (TDF).

The aim of this chapter is to present a review of all the available (either already published or in phase of development) algorithms. Form and characteristics of the algorithms are either recalled or presented, discussing their field of application. Performance and efficiency of the illustrated algorithms are analyzed and compared using both synthetic and actually measured time series.

The chapter is structured as follows. The algorithms for automatic, real-time detection in deep sea level measurements (i.e. in BPR observations) are recalled in section 2, comparing their ability to meet the requisites set out above. Detection in tidal gauge measurements is discussed in section 3. As far as the detection in wind wave measurements is concerned (section 4), the algorithms based on moving average filters are recalled in section 4.1, whilst those based on time domain digital filters such as FIR or IIR filters in section 4.2. Performance and efficiency of these algorithms are analyzed and compared in section 4.3 using synthetic time series, while observations are made and conclusions drawn in Section 5.

2. Detection in BPR measurements

2.1 The DART algorithm

The tsunami-detection algorithm developed by Mofjeld (1997) under the Deep-ocean Assessment and Reporting of Tsunami (DART) program uses a cubic polynomial to predict disturbing wave patterns. The filtered signal is obtained by subtracting at each new time step the prediction from the observation. The algorithm monitors the actual propagation of a tsunami by checking the amplitude of the filtered signal against a prescribed threshold (TS_{amp}), and therefore belongs to the class of the amplitude-discriminating ones.

The predictions ζ_p are updated every sampling interval (i.e. every 15 s), and the prediction time is set equal to 15 s in the future with respect to the actual time t_i . The polynomial is fitted to p -minute averages $\bar{\zeta}$ (centered at the $p/2$ minute) of observations ζ collected over the preceding three hours and p minutes and can be expressed as

$$\zeta_p(t_{i+1}) = \sum_{j=0}^3 w_j \bar{\zeta}(t_i - 0.5p - 60j) \quad (1)$$

where t_i is the actual time expressed in minutes. The coefficients w_i are calculated by applying the Newton's forward divided difference formula, using the preceding temporal parameters. Mofjeld (1997) suggests setting the time interval p at 10 min so as to:

- a) regularize the polynomial fitting point pattern by filtering out background noise typically recorded by BPRs; and
- b) minimize the extent to which an actually detected tsunami indirectly influences the filtered signal by affecting the observation averages (Mofjeld, 1997).

As already stated, in this case ($p=10$ min) the prediction time is set equal to 15 s in the future with respect to the actual time t_i , i.e. 5 minutes and 15 seconds in the future with respect to the time at which is centered the first average.

As shown by Beltrami (2008), the algorithm's prediction error depends both on the time interval p and on the magnitude of the disturbance to be filtered out. In the absence of background sea-noise, this disturbance is mainly caused by the tide. Departure from a perfectly filtered signal (a zero signal) therefore depends on the measurement location. For example, the filtered signals obtained by testing the algorithm on M_2 tides of equal phase and different amplitudes show a residual oscillation of sinusoidal shape. When p is equal to 10 min, the range of this oscillation (i.e. the prediction error) will be approximately 0.26 % of the tidal one. At a location that experiences a tidal range of 2.0 m, an oscillation with a range of 5.0 mm is therefore expected to persist in the filtered signal.

Whatever the time interval p , fixing all the preceding temporal parameters makes it possible to calculate the w_i coefficients *once and for all* and *a priori*. The implementation of equation

(1) is therefore particularly simple. Furthermore, the coefficients w_i are calculated on the sole basis of temporal parameters. This makes the same set applicable to all BPRs, whatever their location. Such characteristics, together with a filtering performance that is effective from a practical point of view, constitute the algorithm's main strengths.

2.2 The ANN algorithm

Similarly to the algorithm by Mofjeld (1997) that by Beltrami (2008) filters out the astronomical and meteorological tides recorded by a BPR by subtracting at each new time step the prediction from the observation, and monitors the actual propagation of a tsunami by checking the amplitude of the filtered signal against a prescribed threshold (TS_{amp}). Therefore, also this algorithm belongs to the class of the amplitude-discriminating ones.

In order to update the prediction of disturbing fluctuations every 15 s, the ANN algorithm proposed by Beltrami (2008) uses a two adaptive-weight (feed-forward) network characterized by 4 input units plus bias, 6 hidden units plus bias and one output unit ($I_4H_6O_1$). The network's inputs consist of the same p -minute averages $\bar{\zeta}$ of bottom pressure observations ζ as those used by the DART algorithm. These values are preprocessed so as to re-scale them linearly in the range $[0;1]$. The network function can be expressed as

$$\zeta_p(t_{i+1}) = \tilde{g} \left\{ w_b^{(2)} + \sum_{h=1}^6 w_h^{(2)} g \left[w_{bh}^{(1)} + \sum_{j=0}^3 w_{jh}^{(1)} \bar{\zeta}(t_i - 0.5p - 60j) \right] \right\} \quad (2)$$

where t_i is the actual time expressed in minutes, $w_{jh}^{(1)}$ and $w_{bh}^{(1)}$ are the adaptive weights connecting input units and bias to the hidden units, and $w_h^{(2)}$ and $w_b^{(2)}$ those connecting hidden units and bias to the output unit. Moreover, $g(\cdot)$ and $\tilde{g}(\cdot)$ represent the hidden and output unit activation functions. In particular, the logistic-sigmoid and the linear activation functions characterize the hidden units and the output unit respectively.

Unlike the coefficients of the cubic polynomial (1), the adaptive weights of equation (2) result from the network's *supervised learning*. If a time series of actual observations ζ is available, it will be possible to present the network with an input array $[\bar{\zeta}]$ and a corresponding output vector $\{\zeta\}$, i.e. with a *training set*. The adaptive weights $[w]$ result from minimizing the error function chosen to express the difference between the calculated $\{\hat{\zeta}\}$ and the actually observed outputs $\{\zeta\}$. In particular, the network proposed by Beltrami (2008) uses:

- the mean square error (MSE) as the error function (Bishop, 1995);
- the standard back-propagation technique to calculate the MSE derivatives with respect to weights (Rumelhart et al., 1986); and
- the Levenberg-Marquardt optimization scheme for iteratively adjusting the network weights at the end of each *epoch* by means of the calculated derivatives (Levenberg, 1944; Marquardt, 1963; Bishop, 1995).

The way in which the adaptive weights are calculated makes the network performance dependent neither on the time interval p , nor on the observed signal range. Actually, the efficiency of the supervised learning relies totally upon how accurately the training set represents all the possible disturbing fluctuations and their composition. If it succeeds in this, the ANN algorithm error is expected to be nearly zero. This is especially so in the case of disturbing fluctuations consisting of regular wavy patterns such as the tidal one. On the other hand, the network training relies on actual data. This makes the resulting adaptive weights

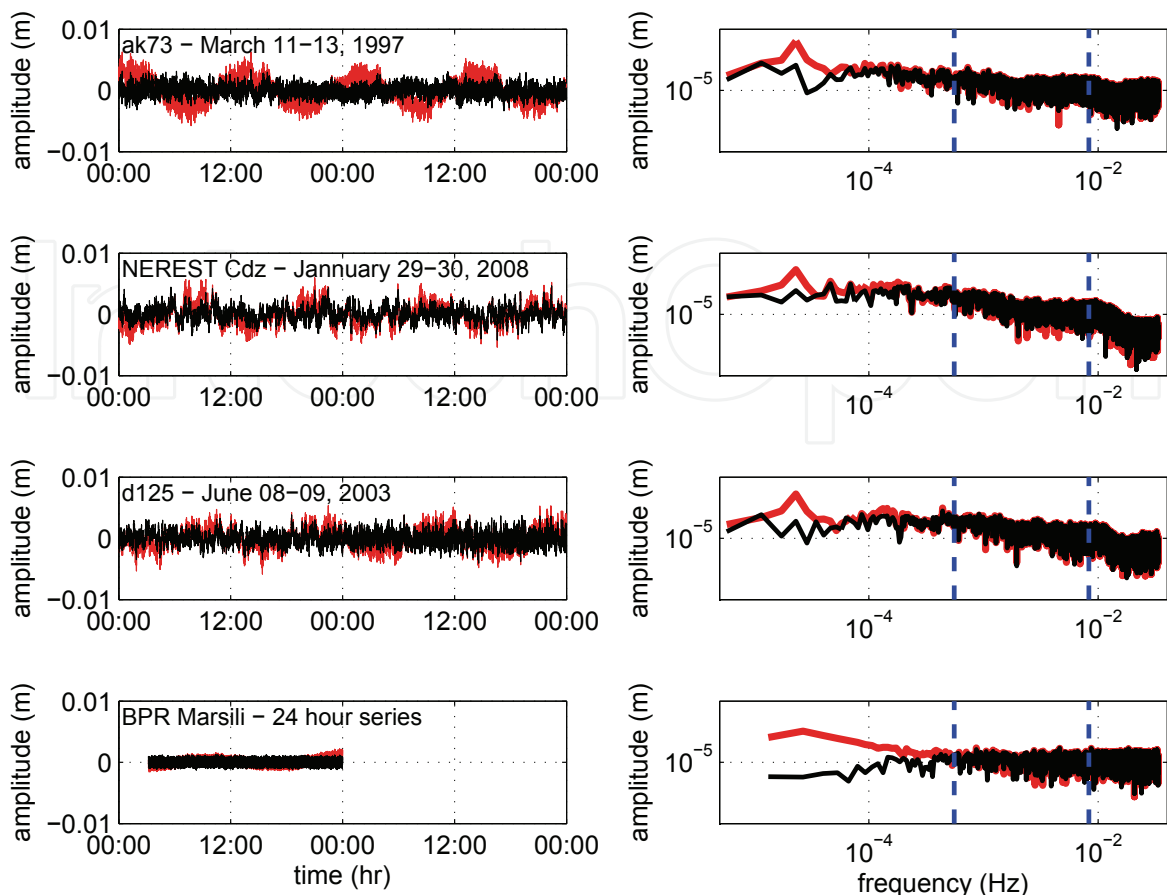


Fig. 1. A comparison of the filtering performance of the DART algorithm (red line) with that of the ANN one (black line). Filtered time series (left graphs) and corresponding amplitude spectra (right graphs). Blue dashed lines in the amplitude spectrum graphs show the limit of the period band 2-30 minutes.

mainly tailored to a specific BPR location. In general, therefore, each BPR is characterized by a specific set of weights, although the same set might be used effectively in different BPRs if their locations are close enough to ensure that the devices are exposed to almost equal tidal and meteorological conditions.

2.3 Filtering and detection performances of DART and ANN algorithms

As far as the filtering performance is concerned, it has been shown (Mofjeld, 1997; Beltrami, 2008) that both the DART and the ANN algorithm are quite effective in predicting, and therefore filtering out, tidal wave patterns. In particular, Beltrami (2008) has shown that the ANN algorithm's closer prediction of both tide and other regular patterns makes it capable of a slightly better filtering performance with respect to the DART algorithm. Such an improvement may be more or less significant, depending on the range of the tide and the characteristics of the background sea noise. In particular, the higher the tidal range at the location of interest (and the lower the background sea noise), the greater the improvement in filtering performance will be. Nevertheless, Beltrami (2008) has also shown that neither the DART nor the ANN algorithm is capable of capturing the feature of the background sea noise. The improved filtering performance that can be achieved using the ANN algorithm therefore relates solely to the astronomical and meteorological tide.

Four different sets of observations (Tab. 1) were analyzed in order to compare the filtering performance of the DART algorithm with that of the ANN one. Two sets were collected during the testing phase of the DART program (retrospective data) by two BPRs (ak73 and d125) respectively deployed in the Northern (Alaska) and Equatorial Pacific (<http://nctr.pmel.noaa.gov/Dart/>). Both the data-sets cover a period of observations of around one year. The third set refers to the observations collected by the BPR deployed in the Gulf of Cadiz (Atlantic Ocean) in the context of the NEAREST program funded by the European Union (<http://nearest.bo.ismar.cnr.it/>). The available set was collected during January, 2008. Finally, a 24-h record of pressure observations collected at a BPR located in the Mediterranean Sea was also analyzed. The considered BPR is located 2040 m below the mean sea level on the slopes of Marsili (a submerged volcano north of Stromboli in the Tyrrhenian Sea).

All pressure data - recorded in either PSIA, mmBar or mH₂O - were firstly converted in Pascals (Pa), and then in meters (i.e. in sea levels) by dividing them for the mean specific (unit) sea-water weight $\bar{\gamma} = \bar{\rho}g$ at the BPR location, being $\bar{\rho}$ the mean sea water density that should be applied in order to make the mean sea level resulting from the recorded data equal to the declared BPR water depth.

Fig. 1 shows the filtered signal resulting from the application of the DART and ANN algorithms (left graphs), and the corresponding amplitude spectra (right graphs). Blue dashed lines in the amplitude spectra show the limits of the period band 2-30 minutes. The ANN algorithm clearly performs better than the DART one in removing regular wave patterns such as the astronomical and the meteorological tide. The amplitude of the components of the ANN filtered signal within the period band 1-26 h ($1 \cdot 10^{-5}$ Hz - $3 \cdot 10^{-4}$ Hz) is invariably lower than that of the components of the DART one. This is particularly evident for the astronomical-tide components with period around 12 h ($2.315 \cdot 10^{-5}$ Hz). These are the components that are responsible for the residual oscillation of sinusoidal shape still present in the signal filtered by the DART algorithm. The amplitude spectra show that neither the DART nor the ANN algorithm is capable of filtering out the components with frequency greater than $3 \cdot 10^{-5}$ Hz. A close prediction of these components is in-fact not possible. Indeed, the components within the period band 2-40 minutes ($4.17 \cdot 10^{-4}$ Hz - $8.33 \cdot 10^{-3}$ Hz) cannot be filtered out using some form of digital filter without removing a possible tsunami.

As far as the detection performance is concerned, it should be noticed that the DART and the ANN algorithm were designed in order to detect an anomaly in the signal resulting from the difference between the observations and the predictions. A tsunami will be detected if the amplitude of such an anomaly is greater than a preselected thresholds. In this regard, both the algorithm guarantee quite an effective detection performance. Nevertheless, although these algorithms can detect a tsunami, they can neither properly identify its waveform nor characterize it in terms of amplitude and period. In other words, neither the DART nor the ANN algorithm can meet the second of the three requisites set out in the introduction.

Station ID	Program	Depth (m)	sample rate (s)	Location	Unit
ak73	DART	4575	15	Alaska	Psia
d125	DART	4500	15	Equatorial Pacific	Psia
cdz	NEAREST	3207	15	Gulf of Cadiz	mmBar
mrs		2040	15	Mediterranean Sea	mH ₂ O

Table 1. Analyzed sets of pressure observations.

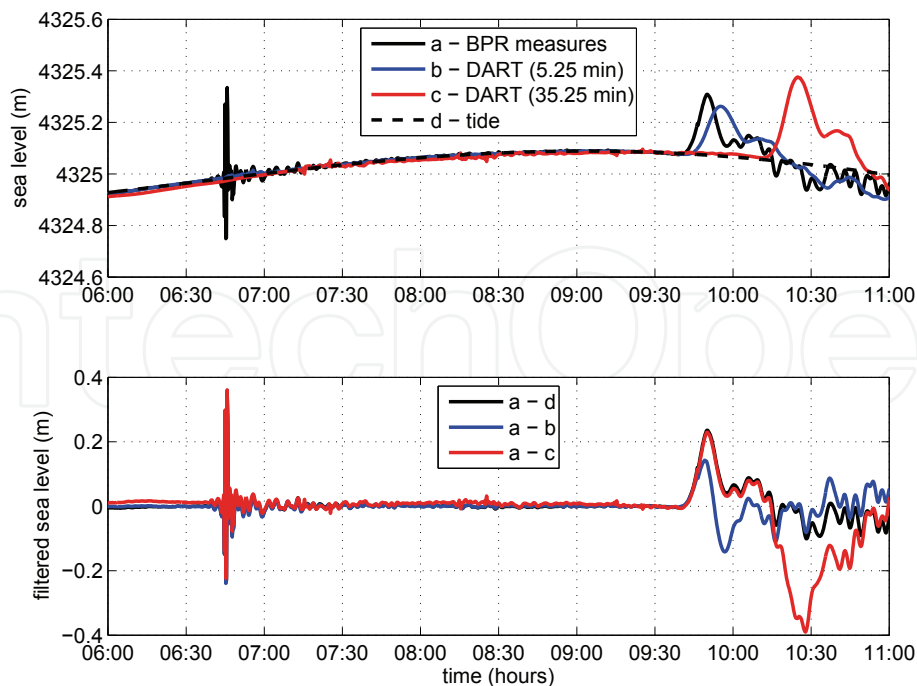


Fig. 2. DART station 32412, February 27, 2010. In the upper graph the actual BPR measurements (black continuous line) are plotted together with DART algorithm predictions (blue and red continuous lines - prediction time respectively set at 5.25 and 35.25 minutes) and the tidal wave (black dashed line) obtained by filtering out from the BPR measurements the components with period lower than 8 hours using a low-pass digital filter. In the lower graph, the de-tided series (black line) is plotted with the series obtained by subtracting the predictions from measurements (blue and red lines).

In order to show this, the data recorded by the BPR of the DART station 32412 (located 630 nautical miles Southwest of Lima, Peru, at a water depth equal to 4325 m) on February 27, 2010 were analyzed. A 8.8 Mw-magnitude earthquake occurred off the coast of the Maule Region of Chile on that date. Following the earthquake, a tsunami was generated, propagating towards the Chilean coasts and spreading in the Pacific.

Pressure data - recorded in PSIA and displayed in meters of water mH_2O - were downloaded from the DART program official site (<http://nctr.pmel.noaa.gov/Dart/>). The data are available with a sampling interval equal to 1 min. A spline was therefore fitted to the original time series in order to synthesize a series with a sampling rate of 15 s.

The data recorded between 06:00 and 11:00 UTC on February 27, 2010 are shown in the upper graph of Fig. 2 by a black continuous line. As before, pressure data were converted in sea level data (i.e. in meters) by dividing them by the mean local specific sea-water weight $\bar{\gamma} = \bar{\rho}g$. At 06:40 UTC, Rayleigh waves are evident in the recorded signal. The propagating tsunami arrived at the BPR location around 09:40 UTC, reaching its maximum amplitude (around 0.24 m over mean sea level) around 09:50 UTC. In the graph, the black dashed line refers to the tidal wave. These data were obtained by filtering out the components with period shorter than 8 hours from the original record. The blue continuous line represents the DART algorithm prediction, being the prediction time set equal to 5.25 minutes (i.e. 15 s in the future with respect to the actual time). As it can be noticed, after few minutes, the DART predictions tend to follow the observations. This is due to the fact that the tsunami has started to influence the first of the observation averages to which is fitted the cubic polynomial.

The black continuous line in the lower graph of Fig. 2 shows the signal obtained by subtracting the tidal pattern from the recorded data. This is the signal that shows the actual tsunami. The blue continuous line shows the tsunami detected by the DART algorithm, and is obtained by subtracting the DART predictions from the observations. The tsunami reconstructed by the DART algorithm has the form of a N-wave (Tadepalli & Synolakis, 1994). Although the departure from a zero signal represented by this wave is sufficient for detection, i.e. is sufficient to exceed a preselected threshold, the form of the tsunami is not properly reconstructed. This is a consequence of the cubic polynomial prediction, i.e. of the fact that the tsunami has started to influence the first of the observation averages to which is fitted the cubic polynomial. It is to be noticed that, given its characteristics, an equal behavior would be observed in the case of the application of the ANN algorithm.

A possible and simple way to overcome this limit is that of lengthening the DART and ANN algorithm prediction time (Beltrami, 2010). By way of example, setting the prediction time to 30.25 minutes (i.e. 1815 s in the future with respect to the actual time, or 35.25 minutes in the future with respect to the time at which is centered the first average), the resulting DART algorithm predictions take the form of the red continuous line of the upper graph of Fig. 2, while the filtered signal is that represented by the red continuous line of the lower graph. As it is shown by the figure, in this case the algorithm is capable of a close reconstruction of the tsunami, at least within the interval of the prediction time (i.e. 30 minutes). It is to be stressed that, in the case of the DART algorithm, such a lengthening has the cost of augmenting the already seen residual oscillation of sinusoidal shape. When the prediction time is set equal to 30.25 minutes the range of this oscillation (i.e. the prediction error) will be approximately 2.54 % of the tidal one. The ANN algorithm with a lengthened prediction time should be therefore preferred at a location that experiences a considerable tidal range.

Clearly, if the prediction time is set equal to 30.25 minutes, equations (1) and (2) will be expressed accordingly, and either the coefficients w_i of the DART algorithm (Tab. 2), or the adaptive weights of the ANN one will be calculated considering this temporal parameter.

3. Detection in TG measurements

Tidal gauges, although important in the context of tsunami detection, cannot be the main devices on which rely a Tsunami Early Warning System (TEWS). In-fact, these gauges are located at the coast, usually within harbor basin, and therefore can be damaged or swept away by the outgoing wave before the onslaught of the first tsunami wave. Furthermore, their readings can be complicated by shape and size of the basins where they are located.

Nevertheless, although affected by these limitations, tidal gauges can be undoubtedly useful for confirming that a coast has been actually hit by a tsunami (and therefore provide a warning to places further away), and for a post-processing analysis of the tsunami's characteristics.

Coefficient	Prediction time 5.25 min	Prediction time 35.25 min
w_0	+ 1.16818457031250	+2.45603613281250
w_1	- 0.28197558593750	-2.72678027343750
w_2	+ 0.14689746093750	+1.67295214843750
w_3	- 0.03310644531250	-0.40220800781250

Table 2. The DART algorithm's coefficients for different settings of prediction time (sampling interval equal to 15s).

Therefore, provided that the sea level is continuously monitored with a suitable sampling interval (≤ 1 minute), they should be equipped in order to perform the automatic, real-time detection of possible tsunamis.

Algorithms for real-time detection of tsunamis in coastal TG measurements were developed for the US network (Mero, 1998), and for the gauges located in British Columbia, Canada (Rabinovich and Stephenson, 2004). As far as the DART and ANN algorithm are concerned, the second one may be effectively used for real-time detection in TGs measurements. As shown by Beltrami (2008), a convenient choice of the training set can actually make the ANN algorithm capable of predicting not only the 'disturbance' due to the astronomical tide, but also other regular disturbing wave patterns such as the meteorological tide and the gravitational normal modes of the harbor basins (i.e. the harbor seiches).

Tinti et al. (2009) and Bressan & Tinti (2010) have proposed a further algorithm that could be useful in order to perform the automatic, real-time detection of a tsunami in tidal gauge measurements. The Tsunami Early Detection Algorithm (TEDA) has been presented at the EGU General Assembly 2010, but has not been published yet. The reader is referred to the available abstract (Bressan & Tinti, 2010) and presentation (Tinti et al., 2009) for more information.

4. Detection in WWG measurements

4.1 Algorithms based on moving-average filters

Two algorithms based on moving-average filters have been already presented. That by McGehee & McKinney (1996) and that used by the DPC (Dipartimento della Protezione Civile - Italian department for civil protection) within the Stromboli's TEWS (Leva, 2004).

The algorithm by McGehee & McKinney (1996) relies on the assumption that a tsunami is defined as an unusually large change in the mean sea surface slope. In this regard, the algorithm belongs to the class of the slope-discriminating ones. The algorithm works as follows. The filtered sea-level $\hat{\zeta}(t_i)$ is obtained by taking the arithmetic mean of the vector $\{\zeta\} = \{\zeta(t_i), \dots, \zeta(t_{i-n+1})\}$ consisting of n samples collected in the time interval defined by the duration Δt of the averaging window. It is clear that n is equal to $\Delta t \cdot f_s$, being f_s the sampling frequency. The averaging window is slid forward by an increment $s\Delta t_s = s/f_s$ (with s an integer value), and the slope of the filtered sea-level between successive intervals is calculated. A tsunami will be triggered if the absolute value of the calculated slope exceeds a preselected threshold TS_{slp} for some m number of successive intervals $s\Delta t_s$. The filter on which is based the algorithm therefore belongs to the class of causal moving-average digital filters which produce a linear phase alteration.

The choice of the values of the algorithm parameters is clearly site dependent, since it depends on both the wind-wave climate and the tidal range at the WWG's location. The issue is clearly a trade-off between opposite demands. The duration Δt of the averaging window should be long enough to filter out the effects of wind waves on the mean. The longer this window duration - and therefore the better the filtering performance - the higher the period of the shorter detectable tsunami. The lower bound of the band of the detectable-tsunami periods is, in-fact, determined by the value chosen for Δt . The upper bound depends on the amplitude of the minimum tsunami to be detected. Given this amplitude, the upper bound period should make the slope of the tsunami steeper than that of the steepest tidal wave measured at the location of interest. As far as the increment $s\Delta t_s$ is concerned, too short a value may lead to a not measurable change in the slope between successive windows for an event of interest, while too long a value may lead to a not usable warning (i.e. a late warning). Finally, the

<i>parameter</i>	<i>value</i>	<i>units</i>
Δt	180-600	s
$s\Delta t_s$	10-50	s
m	1- 4	
TS_{slp}	0.25-1	mm/s

Table 3. Values for the algorithm parameters suggested by McGehee & McKinney (1996) in the case of a sampling frequency equal to 2Hz.

threshold TS_{slp} should be small enough to detect the minimum tsunami considered a threat, and large enough to reject usual changes in slope, as well as unusual but not-threatening ones. Table 3 shows the range of values suggested by McGehee & McKinney (1996) in the case of $f_s=2$ Hz. These values stems out from the assumptions that: (i) the range of the maximum peak period of the wind-waves observed at the generic location of interest is equal to 18-60 s (the duration Δt is therefore on the order of 10 times this period); (ii) the range of the semi-diurnal tide at the same location is on the order of 10 m; and (iii) the amplitude of the minimum tsunami to be detected is equal to 0.5 m. These assumptions constrain the period of the tsunami to be detected to the band 10-40 minutes.

The algorithm used by the DPC (Dipartimento della Protezione Civile - Italian department for civil protection) within the Stromboli's TEWS is characterized by a *cascade* of filters belonging to the class of causal moving-average digital filters and producing a linear phase alteration (Leva, 2004). In particular, given the SPT's sampling interval (0.5 s), it works as follows. A vector $\{\zeta\}$ consisting of the 120 samples collected during the preceding 60 s (i.e. $\{\zeta(t_{i-1}), \dots, \zeta(t_{i-120})\}$) is updated at each time step t_i . The arithmetic mean $\bar{\zeta}$ of this vector is computed and updated every 60 s. This arithmetic mean is subtracted from each new sample $\zeta(t_i)$ in order to filter out tidal oscillations from the signal. The result $\zeta'(t_i) = \zeta(t_i) - \bar{\zeta}$ of this subtraction is stored in the vector $\{\zeta'\} = \{\zeta'(t_i), \dots, \zeta'(t_{i-29})\}$, consisting of the 30 values stored during the last 15 s. The filtered sea-level $\hat{\zeta}(t_i)$ at each new time step t_i is then obtained by taking the mean $\bar{\zeta}'_i$ of $\{\zeta'\}$. The duration of the wind-wave filtering window is therefore equal to 15 s. A tsunami will be triggered if $|\hat{\zeta}(t_i)|$ exceeds a preselected threshold TS_{amp} . The algorithm therefore belongs to the class of the amplitude-discriminating ones.

Given the duration of the filtering window, such an algorithm has a poor performance in removing wind-waves. Nevertheless, it is important to stress that this algorithm was specifically designed for the TEWS operating at the island of Stromboli. In other words, this algorithm was designed for detecting (within measures taken, close to the source, at water depths around 10-20 m) a tsunami generated by a fast-falling landslide detached from the 'Sciara del Fuoco'. To be actually threatening such a tsunami should have - close to the source - an amplitude of several meters and a period from some tens of seconds to few minutes Di Risio et al. (2009). The detection of a tsunami characterized by such an amplitude is not influenced by the residual noise present in the filtered signal resulting from the application of the DPC's algorithm.

4.2 Algorithms based on time-domain, finite or infinite impulse response, digital filters

4.2.1 The algorithm by PARI

The algorithm by PARI (Port and Airport Research Institute of Japan) has been developed in order to perform the automatic, real-time detection of a tsunami in the sea-level measurements collected by both the Doppler-typed Wave Directional Meters (DWDM), and the newly

developed GPS buoy system (Nagai & Shimizu, 2009) of the Japanese Nationwide Ocean Wave information network for Ports and HARbourS (NOWPHAS).

In order to filter out wind-wave components, the algorithm (Shimizu et al., 2006) uses a finite impulse response (FIR) time domain digital filter (TDF) which relies on the direct use of a Hamming window as impulse response. The filter length is fixed to 120 s. Therefore, given the sampling frequency f_s , it spans $2M + 1 = 120 \cdot f_s + 1$ samples. Such a length implies that an output delay of 60 s with respect to the actual time should be accepted in order to make the filter physically realizable (causal). Indeed, this is usual for a FIR filter for which half of the impulse response should be applied to samples collected after the filtered one. At the actual time step t_i , the output of the filter therefore refers to time step $t_j = t_{i-M}$ ($M = 60 \cdot f_s$), and can be expressed as

$$\zeta'(t_j) = \zeta'(t_{i-M}) = \sum_{k=-M}^{+M} h_k \zeta(t_{j-k}) \quad (3)$$

where $\zeta(t)$ is the measured signal, and $\{h\}$ the set of invariant weights known as impulse response. As already stated, Shimizu et al. (2006) suggest the use of a normalized Hamming window as impulse response.

$$h_k = A \left[0.54 + 0.46 \cos \left(\frac{2\pi k}{2M+1} \right) \right] \quad (4)$$

where $-M \leq k \leq +M$, and

$$A = \frac{1}{\sum_{k=-M}^{+M} 0.54 + 0.46 \cos \left(\frac{2\pi k}{2M+1} \right)} \quad (5)$$

is a constant value used to normalize the output signal level.

Fig. 3 shows the gain or magnitude response function $G(f)$ of the FIR-TDF. The figure shows that $G(f) \simeq 1$ for $f < 1/1000$ Hz, i.e. the filter leaves unchanged the components with periods longer than 1000 s. On the other hand, the components with $1/1000 \text{ Hz} \leq f \leq 1/60 \text{ Hz}$ are increasingly attenuated, while those with $f > 1/60 \text{ Hz}$ completely removed from the signal. The FIR-TDF therefore makes the algorithm by PARI capable of detecting and completely characterizing tsunamis with periods greater than 16 minutes (i.e. about 1000 s). Tsunamis with periods ranging from about 16 minutes down to 1 minute, although still detectable, are progressively less characterizable in terms of both amplitude and period.

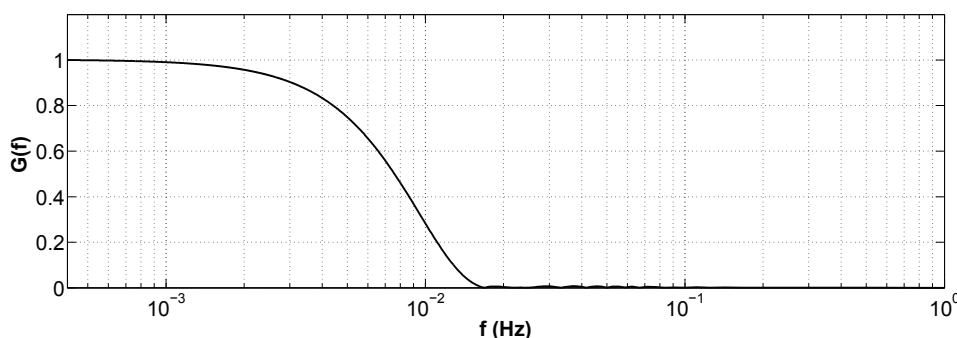


Fig. 3. Magnitude response function $G(f)$ of the windowed FIR-TDF with length equal to 120 s (sample frequency equal to 2Hz).

In order to filter out the astronomical tide, Shimizu et al. (2006) propose to subtract its harmonic prediction $\zeta_p(t_j)$ from the output $\zeta'(t_j)$ of the FIR-TDF. In particular, it is suggested to carry out such a prediction by using the main four tidal constituents resulting from the harmonic analysis of a 6-day record of previous measurements. Relying on harmonic analysis clearly makes the algorithm site dependent.

The filtered sea-level $\widehat{\zeta}(t_j)$ at each new time step t_i is finally obtained by carrying out a moving-average analysis (with one- or half-day time scale) of the resulting signal $\zeta''(t) = \zeta'(t) - \zeta_p(t)$. Such an analysis is suggested in order to correct the mean sea level filtering out the meteorological tide (see Shimizu et al., 2006). As in the case of the DPC algorithm, the algorithm by PARI belongs to the class of the amplitude-discriminating ones. Therefore, it monitors the actual propagation of a tsunami by checking the amplitude of the filtered sea-level against a prescribed threshold (TS_{amp}). In other words, a tsunami will be triggered if $|\widehat{\zeta}(t_j)|$ exceeds such a threshold.

The FIR-TDF guarantees the actual effectiveness of the algorithm in filtering out wind waves. On the other hand, the shorter the period of the tsunami, the lower the capability of the algorithm of detecting and fully characterizing it. The algorithm, in-fact, has been mainly designed for detecting long-period tsunamis (>10 minutes), and providing timely warning of the actually approaching ones not influenced by a delay ≥ 60 s between tsunami measurement and detection.

4.2.2 An algorithm based on a IIR-TDF

In order to overcome the constraints shown by the previously recalled algorithms, Beltrami & Di Risio (2010) have proposed a new algorithm based on a *cascade* of causal filters, the main one being an infinite impulse response (IIR) time domain digital filter (TDF). In particular, the causal IIR-TDF on which relies the algorithm uses the Butterworth (1930) approximation of the gain or magnitude response function (e.g. Smith, 1997; Emery & Thomson, 2001; Sheno, 2006). This type of filter has a nonlinear phase response. Therefore, a *bidirectional* filtering (e.g. Smith, 1997) of the considered signal segment has to be applied in order to avoid the output phase shift. The combination of forward and reverse filtering actually produces a zero phase response at the sole cost of doubling the filter execution time.

Given a sampling interval equal to 0.5 s (2 Hz), the algorithm works as follows (Fig. 4). A vector $\{\zeta\}_i = \{\zeta(t_i), \dots, \zeta(t_{i-n})\}_i$ consisting of the n samples collected during the time interval Δt_a is updated at each time step t_i . In order to filter out wind waves, the signal stored in $\{\zeta\}_i$ should be previously lengthened using a fictitious series made of a transition signal $\{\zeta_t\}_i$ and by the mirror of $\{\zeta\}_i$ (see Beltrami & Di Risio, 2010). The procedure of lengthening is necessary in order to reduce the effect of Gibbs' phenomenon (Gibbs, 1899), i.e the presence of a succession of overshoot ripples at both ends of the filtered signal. In the context of real-time tsunami detection this is a major problem since ringing affects the most important part of the filtered signal, i.e. the output at current time. The lengthened signal is stored in vector $\{\zeta'\}_i$ of duration $\Delta t = \Delta t_a + \Delta t_f$, being the duration Δt_f of the fictitious signal given by the sum of the duration of transition and mirror signal $\Delta t_f = \Delta t_t + \Delta t_a$.

A seventh order IIR-TDF, i.e.

$$\zeta''(t_i) = \sum_{k=0}^7 a_k \zeta'(t_{i-k}) - \sum_{h=1}^7 b_h \zeta''(t_{i-h}), \quad (6)$$

is then applied in order to perform the bidirectional filtering of all the samples contained in vector $\{\zeta'\}_i$. In the equation (6), a_k and b_h are the weights or *taps* of the filter. Given the

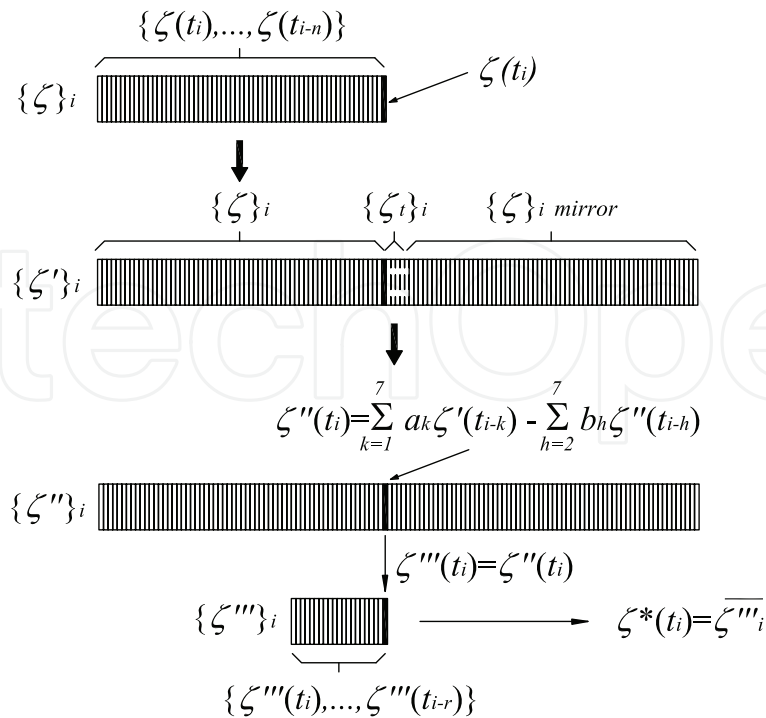


Fig. 4. Proposed algorithm scheme: wind-wave filtering part.

sampling rate and the pass and transition band of the filter, these taps can be calculated *once and for all* and *a priori*. Fig. 5 shows the frequency magnitude response of the chosen IIR-TDF, i.e. a seventh order filter characterized by a pass-band up to 1/60 Hz and a transition band from 1/60 Hz up to 1/30 Hz.

The results of the combination of forward and reverse filtering are stored in vector $\{\zeta''\}_i$. The filtered sample at time t_i , is then extracted from $\{\zeta''\}_i$ and stored in a further vector $\{\zeta'''\}_i = \{\zeta''(t_i), \dots, \zeta''(t_{i-r})\}_i$, consisting of the $(r - 1)$ values obtained in the last r/f_s seconds. At each new time step t_i , the sea-level sample $\zeta^*(t_i)$ filtered for the 'disturbance' due to wind-waves is finally obtained by taking the mean $\overline{\zeta'''_i}$ of $\{\zeta'''\}_i$.

The application of the described part of the proposed algorithm implies a choice for the values of parameters such as the duration of time intervals Δt_a , Δt_t and the number r of samples stored in vector $\{\zeta'''\}_i$. This choice clearly depends on the range of periods of the tsunamis to be detected. By way of example, Tab. 4 shows the values chosen in order to give the algorithm

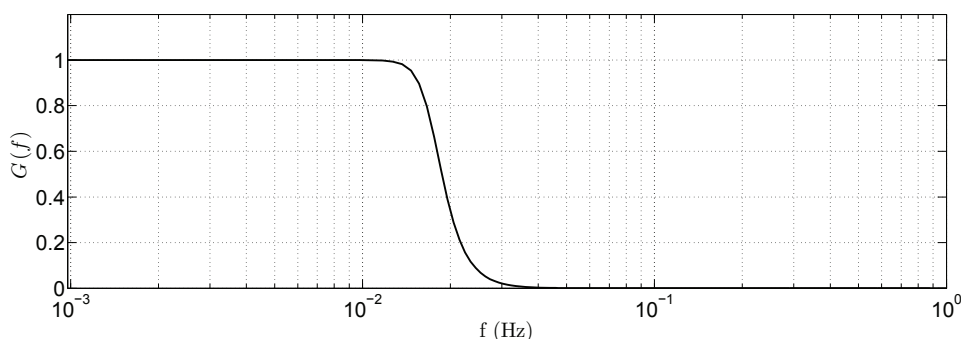


Fig. 5. Frequency magnitude response (gain $G(f)$) of a Butterworth filter with a pass-band up to 1/60 Hz, a transition band from 1/60 Hz up to 1/30 Hz and a filter order $q = 7$.

<i>parameter</i>	<i>value</i>	<i>units</i>
Δt_a	30	minutes
Δt_t	6	s
r	45	samples

Table 4. Values for the algorithm parameters suggested in the case of a sampling frequency equal to 2 Hz.

the wider range of application, i.e. in order to make the algorithm capable of detecting and fully characterizing tsunamis with periods ≥ 60 s.

Either the cubic polynomial on which rely the tsunami-detection algorithm developed by Mofjeld (1997) or the artificial neural network (ANN) proposed by Beltrami (2008) is then used in order to filter out the tidal wave patterns from the signal $\{\zeta^*\}_i$. Given the sampling interval (0.5 s) and an averaging interval $p=10$ minutes, the prediction time is set equal to 35.00833 minutes (i.e. 1800.5 s in the future with respect to the actual time). As shown in section 2.3, this choice makes the algorithm capable not only of detecting a tsunami, but also of characterizing it in terms of both amplitude and period. Clearly, the polynomial coefficients (Tab. 5) or the ANN's weights should be calculated on the basis of the preceding temporal parameters. As already stated, in the case of the cubic polynomial, such a lengthened prediction time has the cost of augmenting the range of the residual oscillation still present in the filtered signal. In particular, the greater the tidal range at the location of interest, the greater the range of the residual oscillation. The ANN algorithm should be therefore preferred at a location that experiences a considerable tidal range. Nevertheless, while the ANN algorithm can guarantee a better filtering for tidal 'disturbance', its implementation makes the overall algorithm site dependent (Beltrami, 2008). Furthermore, at a location that experiences a moderate tidal range, the gain in terms of tidal wave removal from the signal can be masked by the magnitude of the residual noise still present in the signal filtered for wind waves (in particular, in the case of rough and high sea states). In this case, the varied version of the algorithm by Mofjeld (1997) should be preferred.

The tidal wave pattern is filtered out by subtracting at each new time step t_i the polynomial or the ANN output $\zeta_p(t_i)$ from the corresponding sample $\zeta^*(t_i)$. The filtered sea-level at each new time step t_i is therefore expressed as $\hat{\zeta}(t_i)=\zeta^*(t_i)-\zeta_p(t_i)$. As in the case of the DPC and PARI algorithms, a tsunami will be triggered if $|\hat{\zeta}(t_i)|$ exceeds a preselected threshold TS_{amp} . In conclusion, given a sampling frequency equal to 2 Hz and the suggested parameters (Tab. 4), the following data should be stored and progressively updated in the RAM of the measurement device:

1. the 3600 progressively updated measure samples stored in vector $\{\zeta\}_i$;
2. the 7200 progressively updated samples resulting from the lengthening of vector $\{\zeta\}_i$ and stored in vector $\{\zeta'\}_i$;

p (minutes)	10
w_0	+ 2.4432451059353566
w_1	- 2.7008348451980630
w_2	+ 1.6554065948122720
w_3	- 0.3978168555495660

Table 5. Polynomial coefficients for 10-minute averages of observations, $f_s=2$ Hz.

3. the 7200 progressively updated samples stored in vector $\{\zeta''\}_i$ resulting from the bidirectional filtering of the samples stored in vector $\{\zeta'\}_i$;
4. the 44 progressively updated samples stored in vector $\{\zeta'''\}_i$.
5. the 26400 samples filtered for wind-waves (stored and progressively updated in vector $\{\zeta^*\}_i$) during the preceding 3 h and 40 minutes that are necessary to apply the cubic polynomial (or the ANN algorithm), and therefore to filter out tidal wave patterns.

The 4 invariant coefficients of the cubic polynomial (or the 37 ANN weights) and the 15 invariant weights of the IIR-TDF should be clearly stored in the RAM as well. Of course, also the filtered vector $\hat{\zeta}(t_i)$ will be stored, when the filtered signal exceeds the detection threshold TS_{amp} .

4.3 Filtering and detection performances of moving average and time domain FIR or IIR digital filters

A first set of tests was carried out in order to analyze how well the illustrated algorithms remove wind-waves (filtering performance). A total of 6861 different Jonswap wave-spectra, each characterized by a standard peak enhancement factor $\gamma=3.3$ and by a randomly-chosen pair of significant wave height H_{m0} and peak period T_p (Fig. 6), were used to synthesize an equal number of sea-level time-series using the random-phase method (Tuah & Hudspeth, 1982). Each time-series is made of 1024 points, corresponding to a duration of 512 s. No off-set representing the long tidal wave is present in the time-series.

Fig. 7 shows the scatter plots of the maximum amplitude of the filtered signals as a function of the significant wave height H_{m0} of the original synthetic time-series. An upper bound of each scatter corresponding to a specific algorithm has been also assumed and drawn. Given a measurement location characterized by a specific wave climate, such an upper bound gives an indication of the lower threshold that can be selected in the case of amplitude-discriminating algorithms such as that by DPC and PARI, and that based on the IIR-TDF.

Tab. 6 shows the percentages of the maximum amplitude of the filtered signals relative to the significant wave height H_{m0} of the original ones. The table shows that the maximum amplitude of the 'disturbance' still present in the filtered signal is actually only a small fraction of the significant wave height H_{m0} of the original signal, particularly in the case of both the algorithm by PARI, and that based on the IIR-TDF.

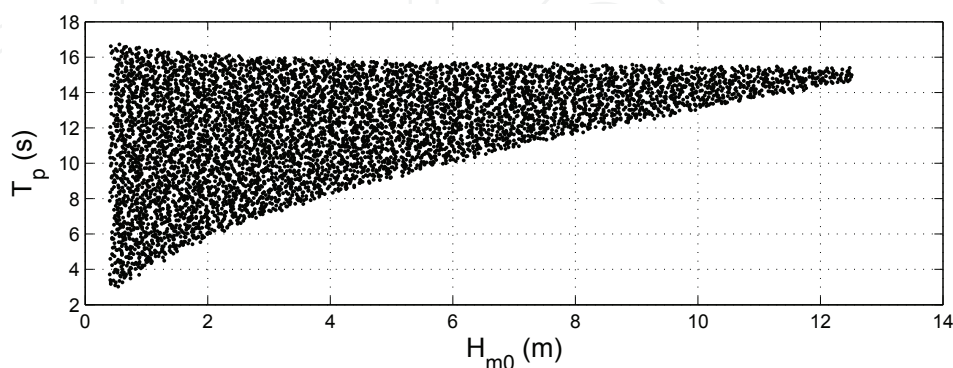


Fig. 6. Scatter plot of the randomly-chosen pair (H_{m0}, T_p) used to characterize 6861 different Jonswap wave-spectra and to synthesize an equal number of wind-wave time series by means of the random-phase method.

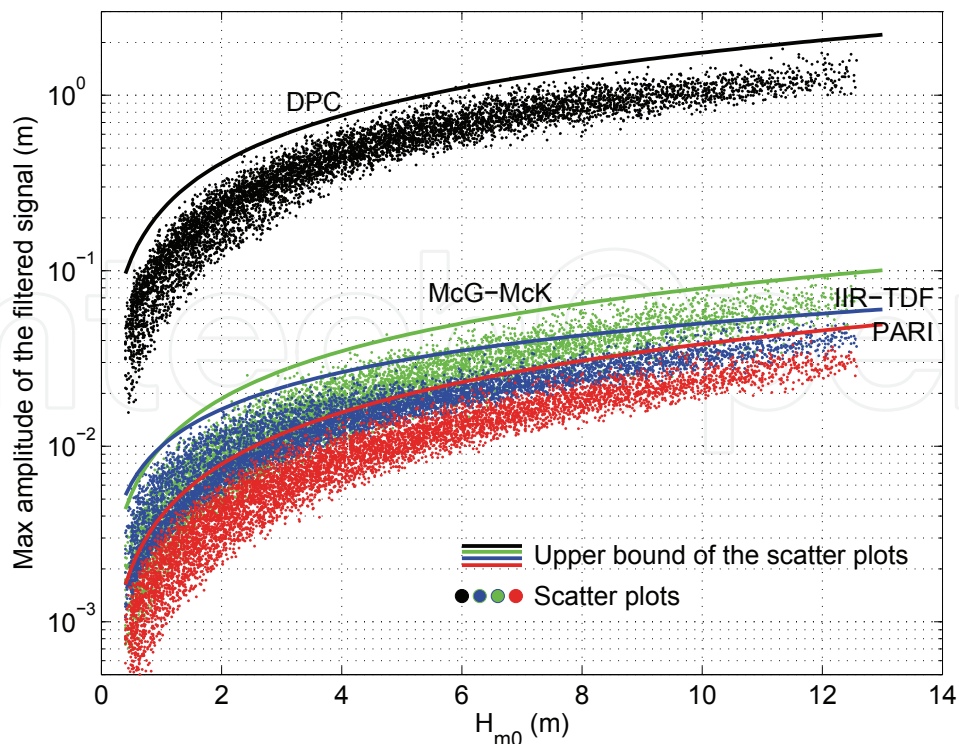


Fig. 7. Scatter plots of the maximum amplitude of the filtered signals as a function of the significant wave height H_{m0} of the original synthetic time-series. Solid lines identify the assumed upper bound of each scatter.

Inspection of both Fig. 7 and Tab. 6 reveals that the best filtering performance is achieved by both PARI and IIR-TDF algorithm. Using these algorithms makes it possible to select a lower threshold TS_{amp} with respect to that needed by the DPC one. In-fact, the lowest detectable tsunami amplitude for PARI and IIR-TDF algorithm will be about 0.05 m, even if the time series characterizes a severe wave climate (i.e. wind-induced significant wave height greater than 10 m). In other words, the algorithm by PARI and that based on the IIR-TDF are equivalent in terms of filtering performance, whilst the one by DPC shows a poor filtering capability. However, as already stated, the DPC algorithm was specifically designed for detecting tsunamis generated by fast-falling landslides detached from the 'Sciara del Fuoco' at Stromboli. To be actually threatening such tsunamis should have - close to the source - an amplitude of several meters, making the wind-wave filtering performance of the DPC's algorithm sufficient. In conclusion, the DPC algorithm can be applied to cases similar to the one of Stromboli, but it can be hardly applied to a more general situation.

$H_{m0} \setminus Alg$ (m)	DPC (%)	McG - McK (%)	PARI (%)	IIR - TDF (%)
1	22.00	1.00	0.40	1.00
3	19.71	0.90	0.39	0.72
6	18.39	0.84	0.39	0.58
9	17.66	0.80	0.38	0.52
12	17.16	0.78	0.38	0.48

Table 6. Percentages of the maximum amplitude of the filtered signals relative to the significant wave height H_{m0} of the original synthetic time-series.

A second set of tests was carried out in order to analyze how well the considered algorithms detect a propagating tsunami within a sea-level signal given by the superposition of a wind-wave and an astronomical tide record. Only the amplitude-discriminating algorithms were considered, i.e. the algorithm by DPC, by PARI, and that based on the IIR-TDF. In-fact, these algorithms will trigger a tsunami if an amplitude threshold TS_{amp} is exceeded. On the contrary, the algorithm by McGehee & McKinney (1996) checks against a prescribed threshold the *slope* of the filtered signal. Therefore, its results are not directly comparable with that of an amplitude-discriminating algorithm. Furthermore, due to its characteristics, it can neither guarantee the characterization of the waveform of the detected tsunami, nor detect tsunamis with period lower than 10 minutes.

Different sinusoidal tsunamis - each characterized by a different amplitude and period - were superposed to different 9 hour-long sea-level time-series, each resulting from the superposition of the same track of the Venice astronomical tide and different wind-wave signals synthesized by means of the random-phase method (Tuah & Hudspeth, 1982). In particular, the method was applied using different Jonswap wave-spectra, each characterized by a standard $\gamma=3.3$, and by a selected significant wave height H_{m0} and a peak period $T_p=4\sqrt{H_{m0}}$.

Figures from 8 to 10 show a selection of the results obtained by performing the real-time analysis of different synthesized sea-level records. Two parameters are particularly useful to assess the detection performance of the algorithms, i.e.

- i) the dimensionless detected-tsunami amplitude a^* expressed as the ratio between the detected \tilde{a} and the actual tsunami amplitude a ; and
- ii) the dimensionless detection delay t^* expressed as the ratio between the detection delay \tilde{t} and the tsunami period T .

It is to be noticed that the detection delay \tilde{t} is defined as the elapsed time between the instants at which the actual and the detected (by the algorithm) tsunami exceed the preselected threshold.

Fig. 8 shows the result of the analysis carried out on a sea-level record resulting from the superposition of the Venice astronomical tide, a wave signal characterizing a slight sea state ($H_{m0}=1.0$ m, $T_p=4.0$ s) and a sine-like tsunami of amplitude $a=0.4$ m and period $T=3.0$ minutes. In this case, the DPC algorithm is still capable of detecting such a small sinusoidal tsunami, and to identify its waveform, at least roughly. Furthermore, the DPC algorithm can spread the alarm 21.5 s after the tsunami starting time (detection delay $\tilde{t}=6.0$ s, dimensionless detection delay $t^*=0.03$). Although still capable of detecting such a small and short tsunami, the PARI algorithm shows a reduced detection performance in terms of both detected tsunami amplitude ($a^*=0.72$) and detection delay ($\tilde{t}=60.0$ s, $t^*=0.33$). In particular, the PARI algorithm can spread an alarm only 75.5 s after the tsunami starting time. As far as the IIR-TDF algorithm is concerned, it is shown to be capable of both a good characterization of the tsunami waveform ($a^*=0.87$) and a timely warning. In-fact, the IIR-TDF algorithm can spread an alarm 37.0 s after the tsunami starting time ($\tilde{t}=21.5$ s, $t^*=0.12$).

Fig. 9 shows the result of the analysis carried out on a sea-level record resulting from the superposition of the same track of the Venice astronomical tide previously used, a wave signal characterizing a very high sea state ($H_{m0}=10.0$ m, $T_p=12.65$ s), and a sine-like tsunami of equal amplitude ($a=0.4$ m) and longer period ($T=8.0$ minutes). Due to its poor filtering performance, the DPC algorithm cannot detect such a small sinusoidal tsunami in this case. On the contrary, both PARI and IIR-TDF algorithm are capable of detecting and characterizing it in terms of

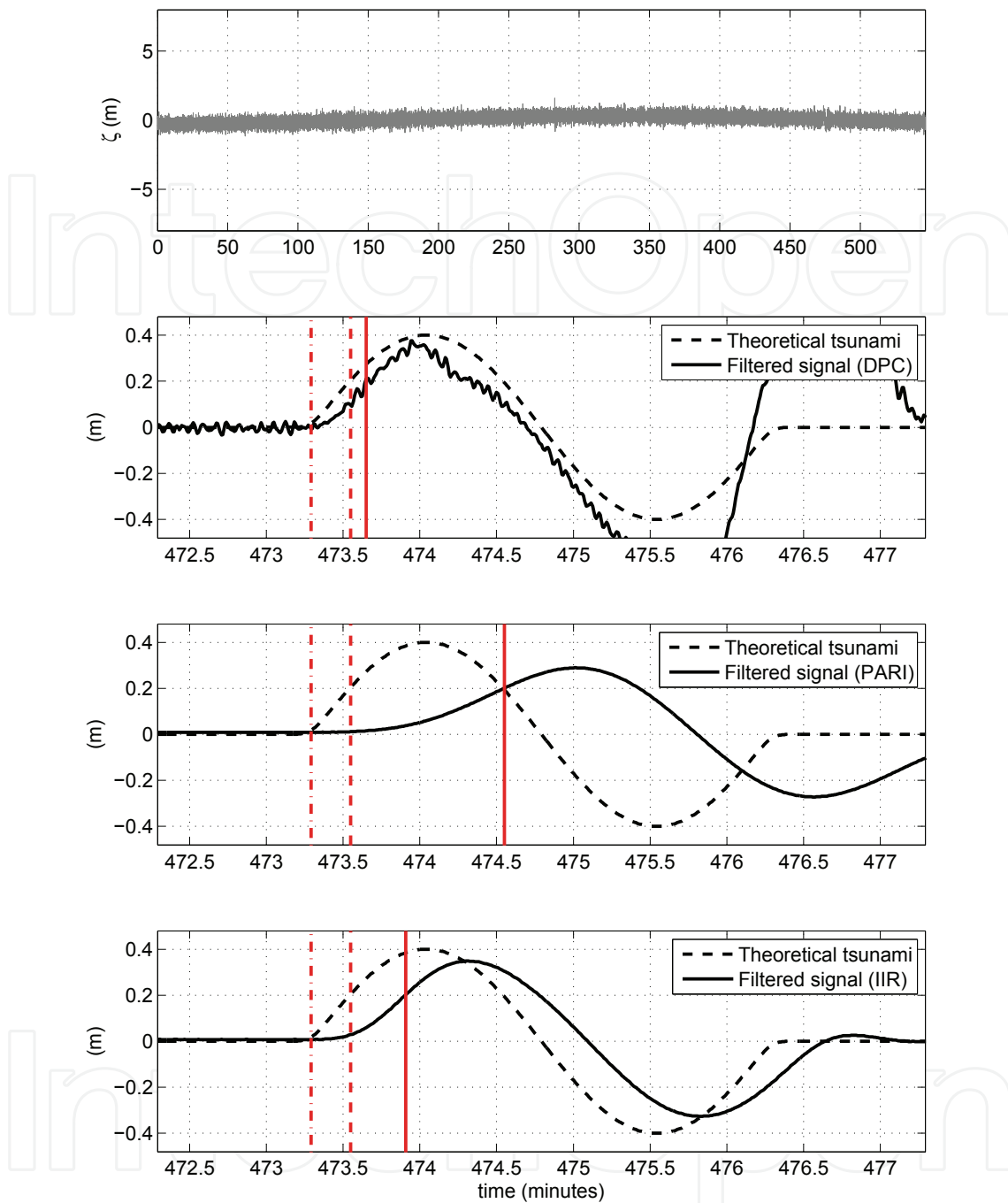


Fig. 8. Upper panel: analyzed sea-level record (resulting from the superposition of Venice tide, a wind-wave signal characterized by a significant height $H_{m0}=1.0$ m and a peak period $T_p=4.0$ s and a sinusoidal tsunami of amplitude $a=0.4$ m and period $T=3.0$ minutes). Lower panels: comparison between the filtered signals resulting from the application of DPC, PARI and IIR-TDF algorithm, and the theoretical sine-like tsunami. Vertical dot-dashed and dashed lines represent the instants at which the sine-like tsunami starts and exceeds the selected threshold respectively ($TS_{amp}=0.2$ m). Vertical continuous line represents the instants at which the filtered signal exceeds the same threshold.

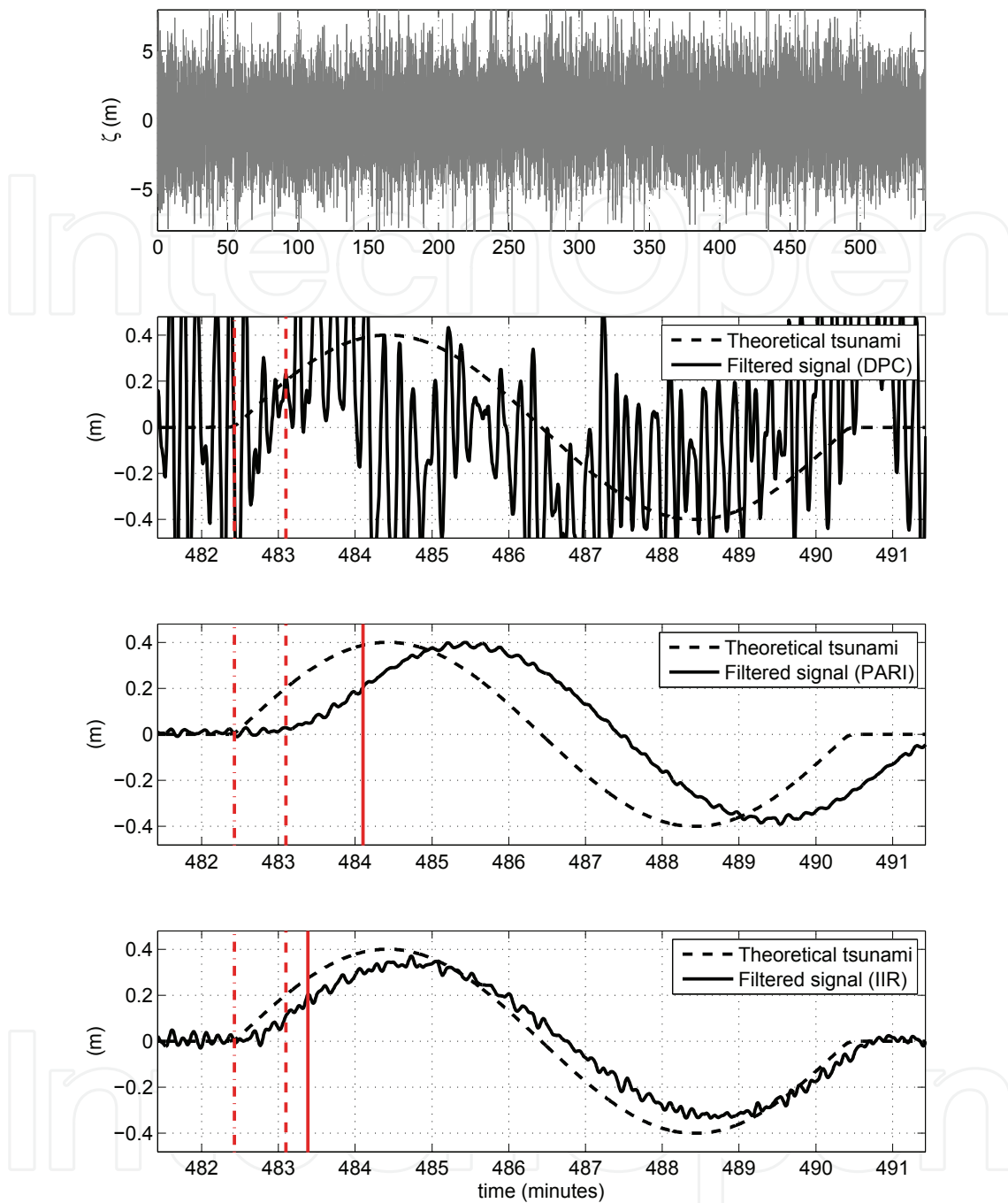


Fig. 9. Upper panel: analyzed sea-level record (resulting from the superposition of Venice tide, a wind-wave signal characterized by a significant height $H_{m0}=10.0$ m and a peak period $T_p=12.65$ s and a sinusoidal tsunami of amplitude $a=0.4$ m and period $T=8.0$ minutes). Lower panels: comparison between the filtered signals resulting from the application of DPC, PARI and IIR-TDF algorithm, and the theoretical sine-like tsunami. Vertical dot-dashed and dashed lines represent the instants at which the sine-like tsunami starts and exceeds the selected threshold respectively ($TS_{amp}=0.2$ m). Vertical continuous line represents the instants at which the filtered signal exceeds the same threshold.

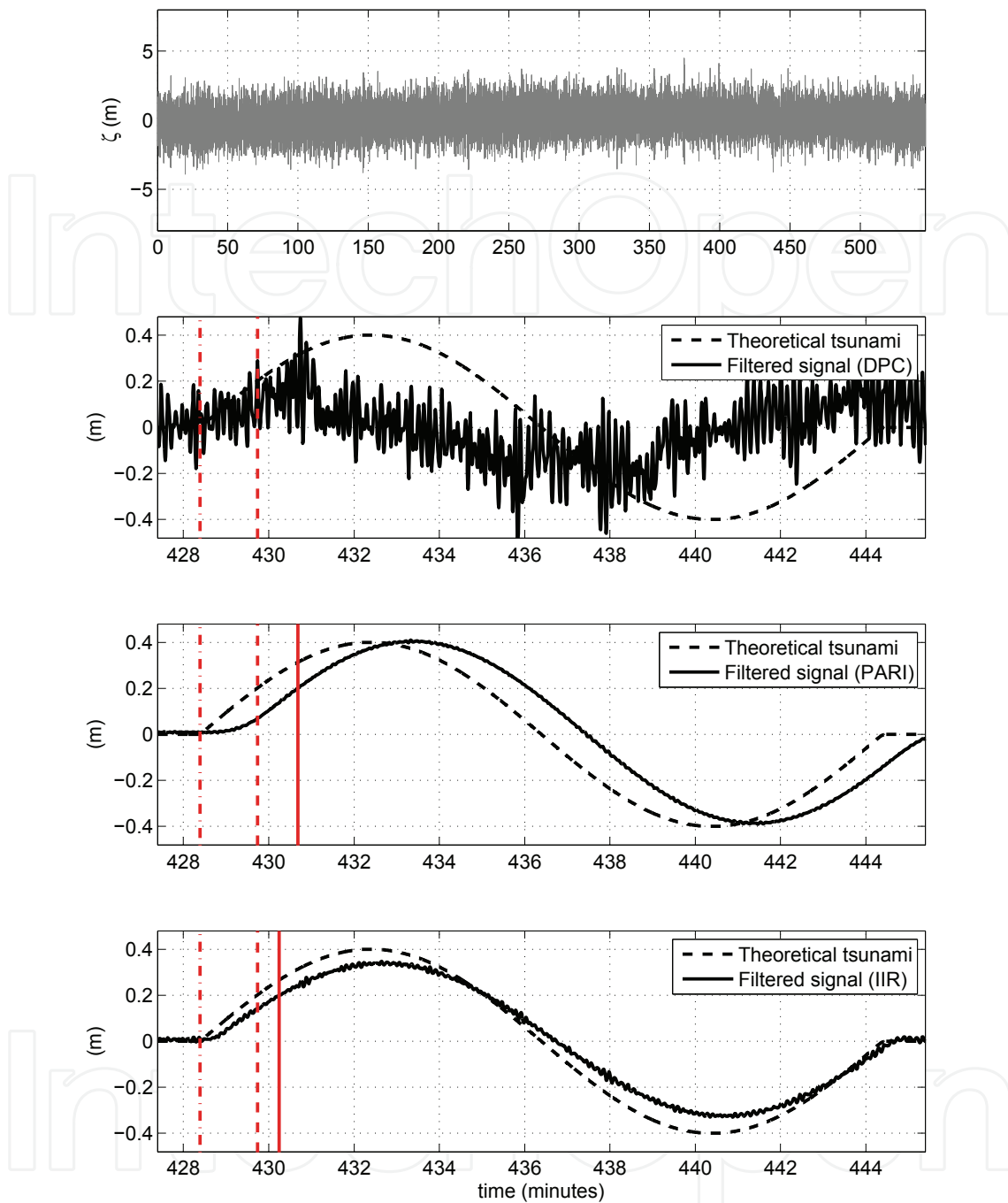


Fig. 10. Upper panel: analyzed sea-level record (resulting from the superposition of Venice tide, a wind-wave signal characterized by a significant height $H_{m0}=4.0$ m, peak period $T_p=8.0$ s and a sinusoidal tsunami of amplitude $a=0.4$ m and period $T=16.0$ minutes). Lower panels: comparison between the filtered signals resulting from the application of DPC, PARI and IIR-TDF algorithm, and the theoretical sine-like tsunami. Vertical dot-dashed and dashed lines represent the instants at which the sine-like tsunami starts and exceeds the selected threshold respectively ($TS_{amp}=0.2$ m). Vertical continuous line represents the instants at which the filtered signal exceeds the same threshold.

amplitude and period. In this regard, a close analysis of the figure shows that the IIR-TDF algorithm has a slightly worst performance with respect to the PARI one in characterizing the tsunami in terms of amplitude. This is due to the mean $\bar{\zeta}^*_i$ that is taken of $\{\zeta^*\}_i$ in order to improve the filtering performance (slightly lower with respect to the PARI algorithm as shown in Fig. 7) of the IIR-TDF algorithm (see par. 4.2.2). On the other hand, the IIR-TDF algorithm shows a better performance with respect to the PARI one in terms of detection delay. In-fact, the detection delay with respect to tsunami starting time is equal to 57.5 s in the case of the IIR-TDF algorithm ($\bar{t} = 17.0$ s, $t^*=0.04$), and equal to 100.5 s ($\bar{t} = 60.0$ s, $t^*=0.13$) in the case of the PARI one.

Finally, Fig. 10 shows the result of the analysis carried out on a sea-level record resulting from the superposition of the Venice astronomical tide, a wave signal characterizing a rough sea state ($H_{m0}=4.0$ m, $T_p=8.0$ s), and a sine-like tsunami of always the same amplitude ($a=0.4$ m) and a longer period ($T=16.0$ minutes). As in the preceding case, the DPC algorithm is not able to detect the sinusoidal tsunami wave, while PARI and IIR-TDF algorithm are. The PARI algorithm appears to closely characterize the sine-like tsunami in terms of both amplitude and period, while the IIR-TDF one shows the already seen and explained reduction in terms of amplitude. As far as the detection delay is concerned, the IIR-TDF algorithm is confirmed to have a better performance than the PARI one. An alarm can be spread 111 s ($\bar{t} = 30.5$ s, $t^*=0.03$) and 137.5 s ($\bar{t} = 57.0$ s, $t^*=0.06$) after the tsunami starting time by using the IIR-TDF or the PARI algorithm respectively.

The illustrated examples allow to catch the peculiarity of each algorithm. The higher the tsunami period, the better the performance of the PARI algorithm with respect to the IIR-TDF one in terms of characterization of the tsunami waveform. This is particularly true for tsunamis of period greater than 10 minutes. On the other hand, the IIR-TDF algorithm is shown to be capable of detecting and almost effectively characterizing tsunamis with a wider range of periods. In-fact, the IIR-TDF algorithm is capable of an effective detection of tsunamis with period greater than 1 minute. Therefore, the IIR-TDF algorithm shows a wider field of application. Furthermore, in terms of detection delay, the performance of the IIR-TDF algorithm is superior to that shown by the PARI one in all the cases. Such a performance is exceeded by that shown by the DPC algorithm only in the case of mild wave climate. It is to be stressed that the detection delay determines the time at which an alarm can be spread, and therefore the elapsed time between the tsunami warning and arrival at the coast of interest. As already stated, this parameter will be essential when tsunamis may be generated either 'at' or 'near' the coast of interest.

5. Conclusion

The present chapter has presented a review of the algorithms to be implemented in the software of either bottom pressure recorders (BPRs), or tidal (TGs) or wind wave gauges (WWGs) in order to automatically perform the automatic, real-time detection of a possible tsunami within recorded signals. In-fact, although a great effort has been recently undertaken by the scientific and engineering community in developing new technologies capable of increasing the awareness of potential tsunamis, at present direct detection in sea level measurements is still the main mean to confirm the actual generation and propagation of a tsunami.

When the tsunami sources are far away from the coast of interest, it will be convenient to collect sea-level measurements far out at sea, between these sources and the coast at risk. Such a location implies great water depths, and makes bottom pressure recorders

(BPRs) with autonomous power supply the more suitable devices to be used. Two already published algorithms can be used in order to perform the automatic, real-time detection in measurements collected by these devices, i.e. the one developed by Mofjeld (1997) under the NOAA's DART program, and that proposed by Beltrami (2008) and based on an ANN (artificial neural network). Comparing the two algorithms makes it possible to show that the ANN one (Beltrami, 2008) is capable of a closer prediction of both tide and other regular patterns and therefore of a slightly better filtering performance. Such an improvement may be more or less significant, depending on the range of the tide and the characteristics of the background sea noise. In particular, the higher the tidal range at the location of interest (and the lower the background sea noise), the greater the improvement in filtering performance will be. As far as the detection performance is concerned, both the DART and the ANN algorithm can detect a tsunami. Nevertheless, these algorithms can neither properly identify its waveform nor characterize it in terms of amplitude and period. In this regard, it has been shown that a possible and simple solution consists in lengthening the algorithms' prediction time. A possible alternative to the DART and ANN algorithm may be the algorithm by Pignagnoli et al. (2010). Nevertheless, although presented at the EGU General Assembly 2010, this algorithm has not been published yet.

The use of the measurements collected by tidal gauges is clearly useful both for providing a real-time confirmation that a specific coast has been actually hit by a tsunami and for a post-processing analysis of the tsunami's characteristics. Nevertheless, tsunami detection in tidal-gauge readings may suffer of the gauge location. At present - given a suitable sampling interval (≤ 1 minute) - the best algorithm to perform the automatic, real-time detection of possible tsunamis in this kind of measurements appears to be the ANN one. A possible alternative may be the Tsunami Early Detection Algorithm - TEDA (Tinti et al., 2009; Bressan & Tinti, 2010) presented at the EGU General Assembly 2010, but not published yet.

When tsunamis may be generated either at or 'near' the coast of interest, it will be essential to collect sea-level measurements in close proximity of the sources. Such a location implies water depths in the order of tens of meters, and makes WWGs a suitable and economically convenient choice. In this case, an important issue will be whether or not the source distance from the closest inhabited location makes the elapsed time between the tsunami generation and arrival sufficient to provide a warning. As far as the algorithms designed to detect a tsunami within a WWG's signal are concerned, those already published are that developed by McGehee & McKinney (1996), that used by the Italian Department for Civil Protection (DPC) within the Stromboli's TEWS (Leva, 2004), and that developed by the Port and Airport Research Institute of Japan - PARI (Shimizu et al., 2006; Nagai & Shimizu, 2009). While the first two algorithms are based on a cascade of time domain moving average filters, the third one uses a finite impulse response (FIR) time domain filter (TDF). The algorithm by McGehee & McKinney (1996) and by PARI (Shimizu et al., 2006) are suitable for automatic, real-time detection of tsunamis with periods greater than 10 minutes. On the other hand, that by DPC is limited by its poor performance in removing wind-waves. In order to overcome the constraints of the preceding listed algorithms, Beltrami & Di Risio (2010) have developed a new algorithm based on a cascade of causal filters, the main one being an infinite impulse response (IIR) time domain digital filter (TDF). Basic tests have shown that the IIR-TDF algorithm guarantees the detection for a wider range of tsunami periods, performing effectively both in filtering out the 'disturbance' due to wind-waves from the gauge recorded signal, and in detecting the presence in this signal of a possible tsunami (although its ability to identify the tsunami waveform has been demonstrated to be slightly inferior to that shown

by the PARI algorithm). Furthermore, the IIR-TDF algorithm proposed by Beltrami & Di Risio (2010) is capable of such a detection with a shorter delay with respect to almost all the recalled already existing algorithms, and therefore of spreading the most timely warning.

6. Acknowledgments

The work presented in this chapter was funded partially by the 'Ministero dell'Istruzione, dell'Università e della Ricerca' - MIUR (Italian Ministry for Formation, University and Scientific Research) under the research projects PRIN2004 (prot. 174/2004) and PRIN2007 (prot. 2007MNBEMY), and partially by the 'Dipartimento della Protezione Civile' - DPC (Italian Civil Protection Department).

7. References

- Beltrami, G. M. (2008). An ANN algorithm for automatic, real-time tsunami detection in deep-sea level measurements, *Ocean Engineering* Vol. 35(5-6): 572–587.
- Beltrami, G. M. (2010). Automatic, real-time detection and characterization of tsunamis in deep-sea level measurements. Submitted for publication to *Ocean Engineering*.
- Beltrami, G. M. & De Girolamo, P. (2006). Preannuncio di un evento di maremoto. Parte 1: Identificazione in tempo reale dell'evento, *XXX Convegno di Idraulica e Costruzioni Idrauliche*, Università La Sapienza.
- Beltrami, G. M. & Di Risio, M. (2010). Algorithms for automatic, real-time tsunami detection in wind-wave measurements - Part I: Implementation strategies and basic tests. (Submitted for publication to *Coastal Engineering*).
- Bishop, C. M. (1995). *Neural network for Pattern Recognition*, Oxford University Press.
- Bressan, L. & Tinti, S. (2010). Test of TEDA, Tsunami Early Detection Algorithm, *Geophysical Research Abstracts, EGU General Assembly 2010*, European Geosciences Union, pp. EGU2010–6450–1.
- Butterworth, S. (1930). Theory of filter amplifier, *Experimental wireless & the wireless engineer* 7: 536–541.
- Corsini, A., Farina, P., Antonello, G., Barbieri, M., Casagli, N., Coren, F., Guerri, L., Ronchetti, F., Sterzai, P. & Tarchi, D. (2003). Space-borne and ground-based SAR interferometry as tools for landslide hazard management in civil protection, *International Journal of Remote Sensing* Vol. 27(12): 2351–2369.
- Di Risio, M., De Girolamo, P., Bellotti, G., Panizzo, A., Aristodemo, F., Molfetta, M. G. & Petrillo, A. F. (2009). Landslide generated tsunamis runup at the coast of a conical island: New physical model experiments, *Journal of Geophysical Research* 114: C01009, doi:10.1029/2008JC004858.
- Eble, M. C. & Gonzalez, F. I. (1991). Deep-ocean bottom pressure measurements in the northeast pacific, *Journal of Atmospheric and Oceanic Technology* Vol. 8(2): 221–233.
- Emery, W. J. & Thomson, R. E. (2001). *Data analysis methods in physical oceanography*, Elsevier.
- Gibbs, J. W. (1899). Fourier's series, *Nature* 59: 606.
- Langer, H. & Falsaperla, S. (2003). Seismic monitoring at Stromboli volcano (Italy): a case study for data reduction and parameter extraction, *Journal of volcanology and geothermal research* Vol. 128(1-3): 233–245.
- Leva, D. (2004). Diagramma catena di misura sensore di pressione a Stromboli - Ginostra. (Not published paper - In Italian).
- Levenberg, R. (1944). A method for the solution of certain problems in least squares, *Quarterly*

- of Applied Mathematics* 2: 164–168.
- Marquardt, D. (1963). An algorithm for least-squares estimation of nonlinear parameters, *Journal of the Society of Industrial and Applied Mathematics* 11(2): 431–441.
- McGehee, D. & McKinney, J. (1996). Tsunami detection and warning capability using nearshore submerged pressure transducers - Case study of the 4 October 1994 Shikotan tsunami, *Proceedings of the 4th International Tsunami Symposium, IUGG*, Kluwer Academic Publisher, Boulder, Colorado, pp. 133–144.
- Mero, T.N. (1998). NOAA/National Ocean Service Application of Real-Time Water Levels, in *Proceedings. Ocean Community Conference, The Marine Technology Society Annual Conference*, Vol. 2: November 16-19, 1998, 1036-1039.
- Mofjeld, H. (1997). Tsunami detection algorithm. (Not published paper (http://nctr.pmel.noaa.gov/tda_documentation.html)).
- Nagai, T. & Shimizu, K. (2009). Basic design of Japanese nationwide GPS buoy network with multi-purpose offshore observation system, *Journal of Earthquake and Tsunami* Vol. 3(2): 113–119.
- Pignagnoli, L., Chierici, F. & Embriaco, D. (2010). A new real time tsunami detection algorithm for bottom pressure measurements in open ocean: characterization and benchmarks, *Geophysical Research Abstracts, EGU General Assembly 2010*, European Geosciences Union, pp. EGU2010–10498.
- Rabinovich, A. B. & F.E. Stephenson (2004). Longwave Measurements for the Coast of British Columbia and Improvements to the Tsunami Warning Capability. *Natural Hazards*, Vol. 32, 3, 313-343.
- Rumelhart, D. E., Hinton, G. E. & Williams, R. J. (1986). Learning internal representations by error propagation, in D. J.L. McClelland & the PDP Research Group (eds), *Parallel Distributed Processing: Explorations in the Microstructure of Cognition*, MIT Press, Cambridge, Massachusetts, pp. 318–362.
- Sheno, B. (2006). *Introduction to Digital Signal Processing and Filter Design*, John Wiley and Sons.
- Shimizu, K., Nagai, T., Lee, J. H., Izumi, H., Iwasaki, M. & Fujita, T. (2006). Development of real-time tsunami detection system using offshore water surface elevation data, *Proceedings of Techno-Ocean 2006 - 19th JASNAOE Ocean Engineering Symposium*, p. 24.
- Smith, S. (1997). *The Scientist and Engineer's Guide to Digital Signal Processing*, California Technical Publishing.
- Tadepalli, S. & Synolakis, C. E. (1994). The run-up of n-waves on sloping beach, *Proceedings of Royal Society, London A*(4): 99–112.
- Tinti, S., Bressan, L., Zaniboni, F. & Armigliato, A. (2009). S3-ur9: Development of real-time algorithms for the detection of tsunami signals on sea-level records: Testing and application to PMEL/NOAA (USA) and analysis of ISPRA (Italy) data., *Progetti DPC Convezione 2007-2009 - Progetti Sismologici*. (Not published poster presentation - In Italian).
- Tinti, S., Pagnoni, F., Zaniboni, F. & E. Bortolucci, E. (2003). Tsunami generation in Stromboli Island and impact on south-east Tyrrhenian coasts, *Natural Hazards and Earth System Sciences* Vol. 3: 299–309.
- Tuah, H. & Hudspeth, R. T. (1982). Comparisons of numerical random sea simulations, *Journal of the Waterway Port Coastal and Ocean Division* 108(4): 569–584.



The Tsunami Threat - Research and Technology

Edited by Nils-Axel MÅrner

ISBN 978-953-307-552-5

Hard cover, 714 pages

Publisher InTech

Published online 29, January, 2011

Published in print edition January, 2011

Submarine earthquakes, submarine slides and impacts may set large water volumes in motion characterized by very long wavelengths and a very high speed of lateral displacement, when reaching shallower water the wave breaks in over land - often with disastrous effects. This natural phenomenon is known as a tsunami event. By December 26, 2004, an event in the Indian Ocean, this word suddenly became known to the public. The effects were indeed disastrous and 227,898 people were killed. Tsunami events are a natural part of the Earth's geophysical system. There have been numerous events in the past and they will continue to be a threat to humanity; even more so today, when the coastal zone is occupied by so much more human activity and many more people. Therefore, tsunamis pose a very serious threat to humanity. The only way for us to face this threat is by increased knowledge so that we can meet future events by efficient warning systems and aid organizations. This book offers extensive and new information on tsunamis; their origin, history, effects, monitoring, hazards assessment and proposed handling with respect to precaution. Only through knowledge do we know how to behave in a wise manner. This book should be a well of tsunami knowledge for a long time, we hope.

How to reference

In order to correctly reference this scholarly work, feel free to copy and paste the following:

Gian Mario Beltrami, Marcello Di Risio and Paolo De Girolamo (2011). Algorithms for Automatic, Real-Time Tsunami Detection in Sea Level Measurements, The Tsunami Threat - Research and Technology, Nils-Axel MÅrner (Ed.), ISBN: 978-953-307-552-5, InTech, Available from: <http://www.intechopen.com/books/the-tsunami-threat-research-and-technology/algorithms-for-automatic-real-time-tsunami-detection-in-sea-level-measurements>

INTECH
open science | open minds

InTech Europe

University Campus STeP Ri
Slavka Krautzeka 83/A
51000 Rijeka, Croatia
Phone: +385 (51) 770 447
Fax: +385 (51) 686 166
www.intechopen.com

InTech China

Unit 405, Office Block, Hotel Equatorial Shanghai
No.65, Yan An Road (West), Shanghai, 200040, China
中国上海市延安西路65号上海国际贵都大饭店办公楼405单元
Phone: +86-21-62489820
Fax: +86-21-62489821

© 2011 The Author(s). Licensee IntechOpen. This chapter is distributed under the terms of the [Creative Commons Attribution-NonCommercial-ShareAlike-3.0 License](#), which permits use, distribution and reproduction for non-commercial purposes, provided the original is properly cited and derivative works building on this content are distributed under the same license.

IntechOpen

IntechOpen